Received: Added at production | Revised: Added at production | Accepted: Added at production

DOI: xxx/xxxx

RESEARCH ARTICLE

A two-way coupling 2D-3D hybrid finite element numerical model using overlapping method for tsunami simulation

Guoming Ling*[1] | Junichi Matsumoto[2] | Kazuo Kashiyama[3]

[1]International Research Institute of Disaster Science (IRIDeS), Tohoku University, Sendai, Japan
[2]National Institute of Advanced Industrial Science and Technology (AIST), Tsukuba, Ibaraki, Japan
[3]Department of Civil and Environmental Engineering, Chuo University, Tokyo, Japan

Correspondence
*Guoming Ling, International Research Institute of Disaster Science (IRIDeS), Tohoku University, Sendai, 980-8572, Japan.
Email: ling@irides.tohoku.ac.jp

Present Address
Aza-Aoba 468-1, Aramaki, Aoba-ku, Sendai, Miyagi, 980-8572, Japan

Abstract

This paper describes a 2D-3D hybrid model for tsunami simulations that uses an overlapping method based on an arbitrary grid. A 2D model is used to simulate wave propagation from the source area to the offshore area, and a 3D model is then used to simulate the free surface flow around structures in coastal areas. An overlapping method that satisfies the conservation and compatibility conditions is developed to couple the two models. The shallow water equations are applied for the 2D model, and the Navier-Stokes equations and continuity equations are applied for the flow field of the 3D model. The Allen-Cahn equation is applied for the interface-capturing method of the 3D model. The stabilized finite element method is applied for the spatial discretization and the Crank-Nicolson method is used for the temporal discretization of the governing equations. The model is verified and validated through several numerical analysis examples.

KEYWORDS:
2D-3D hybrid model, overlapping method, two-way coupling, shallow water, free surface flow, finite element method

1 | INTRODUCTION

Since the tsunami disaster following the 2011 Great East Japan Earthquake, awareness of the importance of the predicting the inundation area of the tsunami and the damage to structures has increased considerably. For tsunami simulations, the 2D numerical method based on shallow water theory is particularly popular[1,2,3,4], achieving comparatively high accuracy in predicting wave propagation and the inundation area at relatively low computational cost. However, for the run-up of tsunami waves to structures around urban areas, it is inappropriate to apply the shallow water approximation because it neglects vertical acceleration. Therefore, free surface flow simulations based on the 3D Navier-Stokes equations have been developed[5,6]. Unfortunately, the huge computational cost of such simulations makes it unrealistic to simulate tsunami waves from the source area to urban areas in 3D. Therefore, hybrid models represent an efficient and reasonable tool for simulating ocean wave propagation in 2D and modeling the target area with structures in 3D.

In recent years, various 2D-3D hybrid models have been proposed. The most outstanding ones are described below.

Some 2D-3D hybrid models are based on structured Cartesian grids[7,8,9,10,11]. These models show that 2D-3D hybrids can significantly reduce the computational load compared with fully 3D models, and can also reproduce the characteristics of 3D flows that cannot be reproduced by 2D models. However, as these methods use structured grids, meshing the structure or the terrain with a complex geometry is a difficult part of the numerical simulation. Hence, Takase et al. [12] proposed a 2D-3D hybrid model based on the stabilized finite element method that uses an arbitrary grid. In this model, the multiple point constraint

[0]**Abbreviations:** 2D-3D hybrid model, overlapping method, two-way coupling, shallow water, free surface flow, finite element method

(MPC) method is employed to connect the 2D and 3D models, for which a shared border boundary has to be set between the 2D and 3D domains. The applications presented by the authors were limited to some simple numerical examples. Recently, Mitsume et al.[13] and Asai et al.[14] proposed 2D-3D hybrid models using particle methods, but these are one-way coupling models.

The objective of our study is to develop a 2D-3D hybrid model for large-scale tsunami simulations that can treat complicated geometries in a two-way coupling. The shallow water equations are applied as the governing equations for the 2D model, and the Navier-Stokes equations and continuity equations are applied as the governing equations for the flow field of the 3D model. To increase the precision of the interface for the free surface flow, the Phase-Field Model (PFM) using the Allen-Cahn equation is applied as the interface-capturing method of the 3D model. The PFM approach is compared with the traditional Volume of Fluid (VOF) method[15]. To solve the governing equations, the stabilized finite element method[2] is applied for the spatial discretization and the Crank-Nicolson method is used for the temporal discretization. Several numerical examples are simulated to demonstrate the validity and efficiency of the proposed method.

The remainder of this paper is organized as follows. In Section 2, the governing equations and the numerical schemes of the 2D model are introduced. In Section 3, the governing equations and the numerical schemes of the 3D model are introduced. Section 4 describes the 2D-3D overlapping method for the 2D and 3D models. Section 5 proposes a switch method to increase the efficiency of 2D-3D coupling. Section 6 presents the results of several numerical tests for verification and validation. Finally Section 7 gives some concluding remarks.

2 | 2D SHALLOW WATER MODEL

2.1 | Governing Equations

The wave propagation from the wave source area to the offshore area is governed by the following nonlinear shallow water equations:

$$\frac{\partial(U_i H)}{\partial t} + \frac{\partial(U_j U_i H)}{\partial x_j} + \nu_e \frac{\partial^2(U_i H)}{\partial x_j^2} + \frac{g n^2 U_i \sqrt{U_j U_j}}{H^{\frac{1}{3}}} + gH\frac{\partial(H+z)}{\partial x_i} = 0 \tag{1}$$

$$\frac{\partial H}{\partial t} + \frac{\partial(U_i H)}{\partial x_i} = 0 \tag{2}$$

where U_i, U_j are the horizontal depth average velocity in the x_i, x_j direction, H is the total water depth, g is the gravitational acceleration, ν_e is the eddy viscosity coefficient, n is the Manning's roughness coefficient and z is the depth of the bottom.

2.2 | Numerical Schemes

The Streamline Upwind/Petrov-Galerkin (SUPG) method[2] is applied for the spatial discretization of the governing equations, and the Crank-Nicolson method is used for the temporal discretization. To solve the simultaneous linear equations, the Bi-Conjugate Gradient STABilized (Bi–CGSTAB) method based on element-by-element processing is applied. The Eulerian method[16] is applied as the wetting and drying treatment for run-up simulation.

3 | 3D FREE SURFACE FLOW MODEL

3.1 | Governing Equations

The Navier–Stokes equations **(3)** and the continuity equations **(4)** are written as

$$\rho\left(\frac{\partial u_i}{\partial t} + u_j\frac{\partial u_i}{\partial x_j} - f_i\right) + \frac{\partial p}{\partial x_i} - \mu\frac{\partial}{\partial x_j}\left(\frac{\partial u_i}{\partial x_j} + \frac{\partial u_j}{\partial x_i}\right) = 0, \tag{3}$$

$$\frac{\partial u_i}{\partial x_i} = 0. \tag{4}$$

As one of the most popular interface-capturing method for the free surface flow, the VOF is adopted here as a reference method, and it is governed by the following advection equation:

$$\frac{\partial \phi}{\partial t} + u_j\frac{\partial \phi}{\partial x_j} = 0. \tag{5}$$

where u_j is the advection velocity computed from the flow field. ϕ is the phase function, with $\phi = 1$ denoting fluid, $\phi = 0$ denoting gas, $\phi = 0.5$ denoting free surface.

For a 2D-3D hybrid model, it is very important to get high accuracy water surface elevation especially at the 2D-3D connected interface. Therefore, the PFM is applied in the present model. As a governing equation, the Allen-Cahn equation **(6)**[17,18] is employed:

$$\frac{\partial \phi}{\partial t} + u_j \frac{\partial \phi}{\partial x_j} = -M_a[\xi(\phi) - k_\phi(\frac{\partial^2 \phi}{\partial x_j^2} + \kappa\Big|\frac{\partial \phi}{\partial x_k}\Big|)], \tag{6}$$

where M_a, $\xi(\phi)$, k_ϕ, κ are defined as,

$$M_a = \frac{2b^2}{\delta^2} M\gamma,\ b = 2\tanh^{-1}(1-2\lambda),\ \delta = a_\delta h_\delta, \tag{7}$$

$$\xi(\phi) = \frac{\partial f(\phi)}{\partial \phi},\ f(\phi) = \phi^2(1-\phi)^2, \tag{8}$$

$$k_\phi = \frac{\delta^2}{2b^2}, \tag{9}$$

$$\kappa = \nabla \cdot \mathbf{n},\ \mathbf{n} = \frac{\boldsymbol{\nabla\phi}}{|\boldsymbol{\nabla\phi}|}, \tag{10}$$

where $M, \gamma, \delta, h_\delta, k_\phi, \kappa, \mathbf{n}$ represent the interface mobility, interface energy, continuously changing gas-liquid interface width, representative length of element, gradient coefficient, interface curvature, and interface normal vector. ρ, u_i, f, p, μ are the density, velocity, body force, pressure, and viscosity coefficient, respectively. For the PFM, the density ρ and the viscosity coefficient μ of each node are computed by the follow equations[19]:

$$\rho = \frac{\rho_l + \rho_g}{2} + \frac{\rho_l - \rho_g}{2}\sin\Big[\frac{\phi - (\phi_l + \phi_g)/2}{\phi_l - \phi_g}\pi\Big], \tag{11}$$

$$\mu = \frac{\mu_l + \mu_g}{2} + \frac{\mu_l - \mu_g}{2}\sin\Big[\frac{\phi - (\phi_l + \phi_g)/2}{\phi_l - \phi_g}\pi\Big], \tag{12}$$

For the VOF method, the density ρ and viscosity coefficient μ are defined as

$$\rho = \rho_l\phi + \rho_g(1-\phi), \tag{13}$$

$$\mu = \mu_l\phi + \mu_g(1-\phi). \tag{14}$$

where ρ_l, ρ_g, μ_l, μ_g are the density and viscosity coefficients of the liquid and gas phases, respectively.

3.2 | Numerical Schemes

The SUPG-Pressure Stabilizing/Petrov-Galerkin (PSPG) method[20] is applied for the spatial discretization of the Navier-Stokes equations. SUPG is applied to the advection equation and the Allen-Cahn equation. The Crank-Nicolson method with second order accuracy is used for the temporal discretization of the governing equations. To solve the simultaneous linear equations, the diagonal scaling preprocessing method, element-by-element processing, and Bi-CGSTAB are applied.

4 | THE 2D-3D OVERLAPPING METHOD

In this paper, a 2D-3D overlapping method based on an arbitrary grid is described. The proposed method separates the computational domain into a 2D domain and a 3D domain (see **Figure 1**). The overlap domain for the 2D and 3D domains is then specified. The 2D and 3D domains and meshes can be arbitrary. The inner boundary of the 2D domain is defined as a 2D connection boundary(the red polygon line shown in the figure), while the outer boundary of the 3D domain is defined as a 3D connection boundary(the red rectangular line shown in the figure and the vertical faces at the lines). In the 2D and 3D connection boundary, the 2D and 3D nodes can be located at different places. For the computation, the flow velocities and water

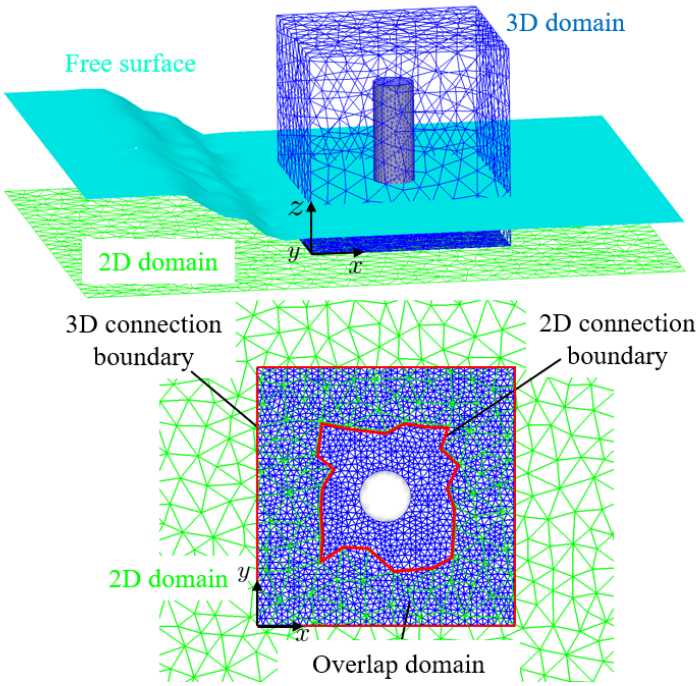

FIGURE 1 Schematic of the meshes using in a 2D-3D overlapping method.

depths computed from the 3D domain are used as the boundary conditions of the 2D connection boundary. Similarly, the flow velocities and water depths computed from the 2D domain are used as the boundary conditions of the 3D connection boundary. For real terrain tsunami simulations, the 3D domain can be located anywhere we require precision computations. Because the positions of the 2D and 3D nodes are different, the boundary conditions of the 2D/3D connection boundary can be computed by interpolation. A flowchart of the 2D-3D overlapping method is shown in **Figure 2**, and it is elaborated by the following.

Firstly, after reading all the input data, the flow velocity u_i^{n+1} and the phase function ϕ_i^{n+1} of step n+1 in the 3D domain are approximated by the following equations:

$$u_i^* = \frac{3}{2}u_i^n - \frac{1}{2}u_i^{n-1}, \tag{15}$$

$$\phi_i^* = \frac{3}{2}\phi_i^n - \frac{1}{2}\phi_i^{n-1}, \tag{16}$$

$$u_i^{n+1} \approx 2u_i^* - u_i^n, \tag{17}$$

$$\phi_i^{n+1} \approx 2\phi_i^* - \phi_i^n, \tag{18}$$

where u_i^*, ϕ_i^* are approximated by the second-order accuracy Adams-Bashforth method.

Secondly, the boundary conditions of the 2D connection boundary are computed by using the results (u_i^{n+1} and ϕ_i^{n+1}) from 3D domain. **Figure 3** shows a cross section of a 2D connection boundary. In this figure, auxiliary nodes S_i (the red dash line nodes) are set the same distance above the nodes of the 2D boundary. We must find which elements (in the 3D domain) the auxiliary nodes belong to. The values of the phase function $\phi_{s_i}^{n+1}$ and the flow velocity $u_{i\,s_i}^{n+1}$ of the auxiliary nodes are computed by interpolating from the tetrahedron elements using the following interpolation equations:

$$\phi_{s_i}^{n+1}(x,y,z) \approx \sum_{\alpha=1}^{4} N_\alpha^e(x,y,z)\phi_\alpha^{n+1}, \tag{19}$$

$$u_{i\,s_i}^{n+1}(x,y,z) \approx \sum_{\alpha=1}^{4} N_\alpha^e(x,y,z)\phi_\alpha^{n+1}. \tag{20}$$

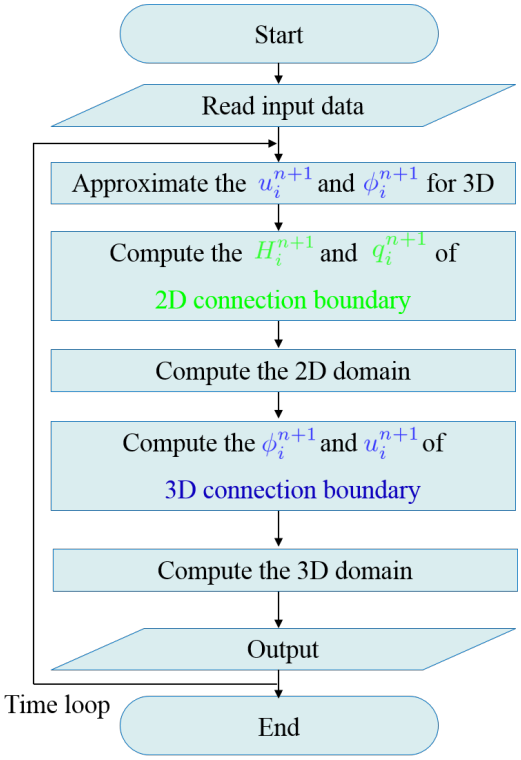

FIGURE 2 Flowchart for the 2D-3D overlapping method.

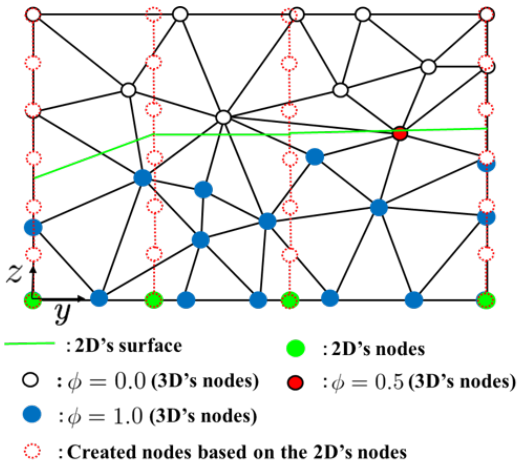

FIGURE 3 Cross section of a 2D connection boundary.

The values of the auxiliary nodes are then substituted into the following integral equations, to obtain the boundary conditions of the 2D connection boundary (see **Figure 4**):

$$H_i^{n+1} = \int \phi_{s_i}^{n+1}(z)dz, \tag{21}$$

$$q_i^{n+1} = U_i^{n+1} H_i^{n+1} = \int \phi_{s_i}^{n+1}(z) u_{i_{s_i}}^{n+1}(z)dz. \tag{22}$$

The 2D domain is then computed using the boundary conditions of the 2D connection boundary.

Thirdly, the boundary conditions of the 3D connection boundary are computed. **Figure 5** illustrates the computation of the phase function at the 3D connection boundary. We compare the water depth H_{2D} with those of the nodes at the 3D connection

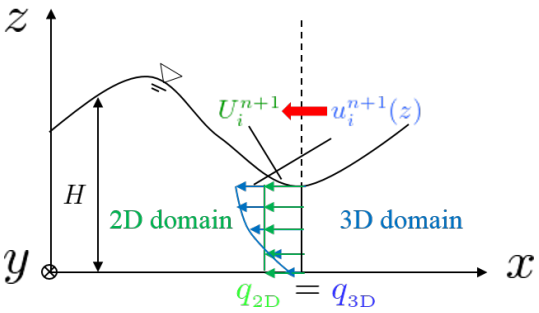

FIGURE 4 Flow rate preservation condition at the 2D connection boundary.

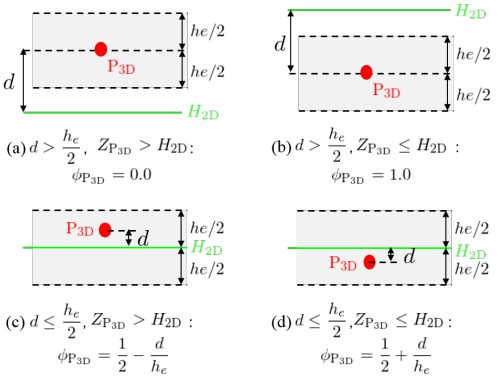

FIGURE 5 Computation of the phase function at the 3D connection boundary.

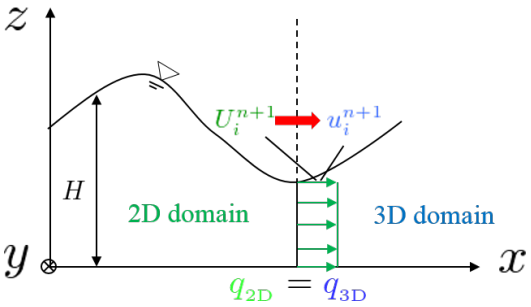

FIGURE 6 Flow rate preservation condition at the 3D connection boundary.

boundary. We consider the four cases shown in **Figure 5**. In the figure, $Z_{P_{3D}}$ is the coordinate value in the vertical direction of a node P_{3D} in the 3D domain. d is the distance from node P_{3D} to the water surface in the 2D domain. h_e is the representative length of the tetrahedron element. The flow velocity for the 3D connection boundary is given by the average flow velocity in the 2D region (see **Figure 6**).

$$u_i^{n+1} = U_i^{n+1}, i = 1, 2, \tag{23}$$

$$u_3^{n+1} = 0. \tag{24}$$

Finally, the 3D domain is computed using the boundary conditions of the 3D connection boundary and the 3D numerical model, the results are output, and the time loop continues.

5 | SWITCH METHOD

For the large-scale simulation, it could take a lot of computational time for wave propagation from source area to an target 3D area, such as a real terrain tsunami simulation. In order to increase the efficiency by reducing computational memory and computational time, a switch method is presented in this section. **Figure 7** shows the conceptual diagram of the switch method. In this method, the water depth H_t is checked at the 3D connection boundary by every step, before the wave coming to the 3D connection boundary ($H_t = H_0$), all the target computational area is computed by the 2D model. When the wave reach the 3D connection boundary ($H_t \neq H_0$), the target computational area is separated into 2D and 3D domain and computed by the 2D-3D hybrid model.

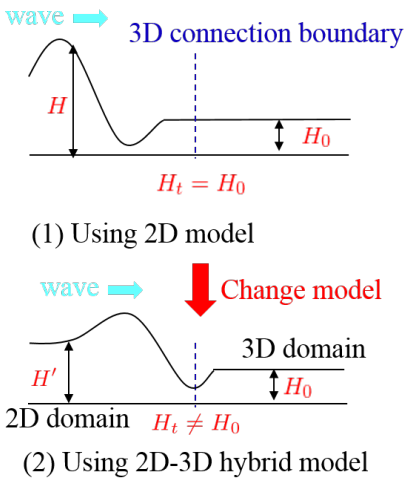

FIGURE 7 Switch Method.

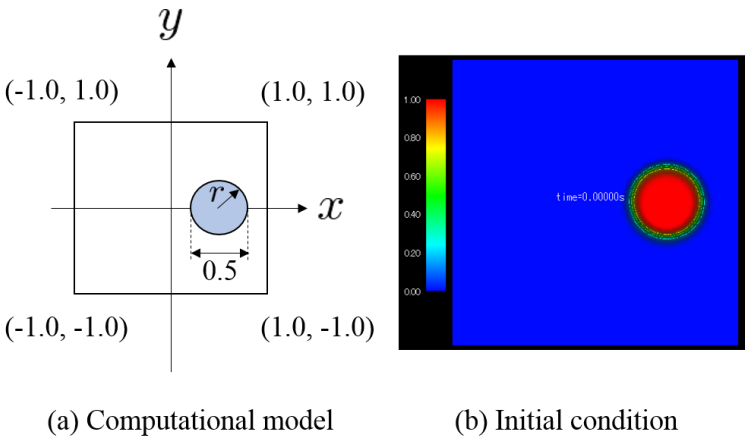

FIGURE 8 Rotating cylinder problem.

6 | NUMERICAL EXAMPLES

6.1 | Rotating cylinder problem

To examine the effectiveness by applying the Allen-Cahn equation instead of the advection equation, we simulated a benchmark problem rotating cylinder (see **Figure 8**). The initial conditions are $\phi = 1$ $(r \leq 0.25)$, $\phi = 0$ $(r > 0.25)$, and $r^2 = (x-0.5)^2 + y^2$. The advection velocity is set as $u_j = (-y, x)$. For the computational conditions, the mesh size is $\Delta x = \Delta y = 1/48$ and the time increment is $\Delta t = \pi/400$. The parameters for the Allen-Cahn equation are set as $a_\delta = 3.0$, $\gamma = 0.0001$.

Figures 9 and **10** show the results after one cycle rotation. From the results, we can see overshoot and undershoot phenomenons especially near the ridges of the cylinder top by using pure advection equation, but these are reduced in the results of the Allen-Cahn equation. In addition, the center cross section of the results by the Allen-Cahn equation is in better agreement with the initial condition than the advection equation as shown in the **Figures 10**.

6.2 | Run-up of solitary wave problem

The run-up of a solitary wave problem (see **Figure 11**) is simulated to investigate the applicability of the 2D-3D hybrid model. Two cases in which the 2D and 3D domains are separated at different positions are considered. For case 1, the structured mesh

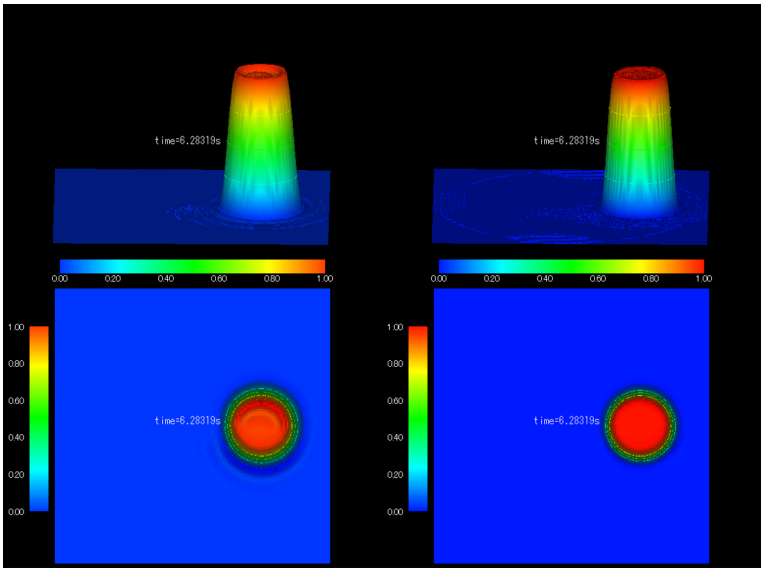

(a) Advection Eq. (b) Allen-Cahn Eq.

FIGURE 9 Computational results (after one cycle).

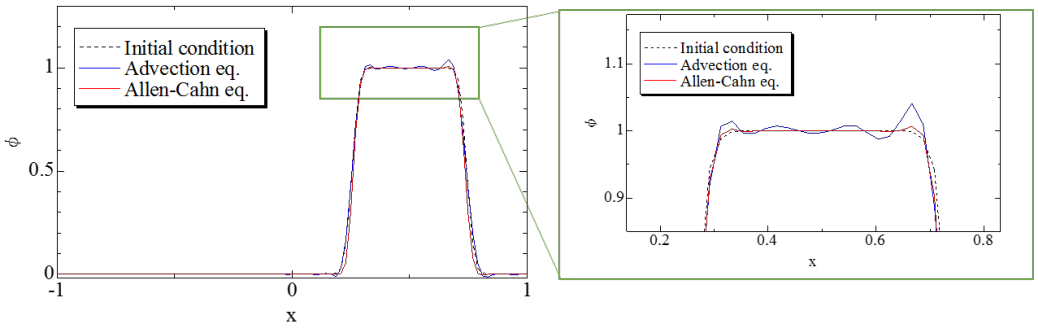

FIGURE 10 Cross section of the cylinder at y=0.

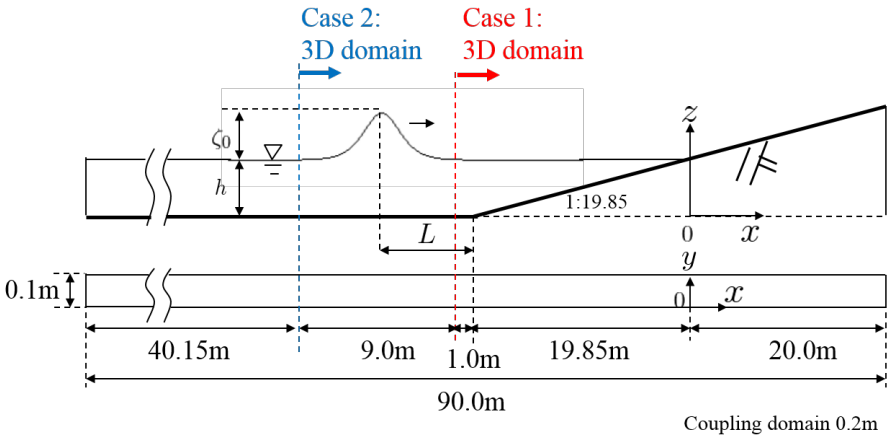

FIGURE 11 Computational model.

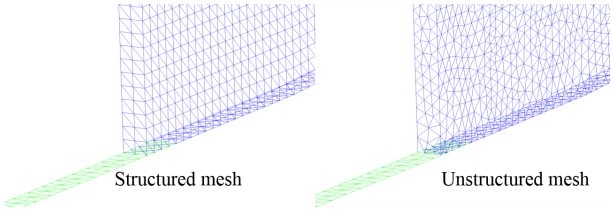

FIGURE 12 Meshes around the connection boundary.

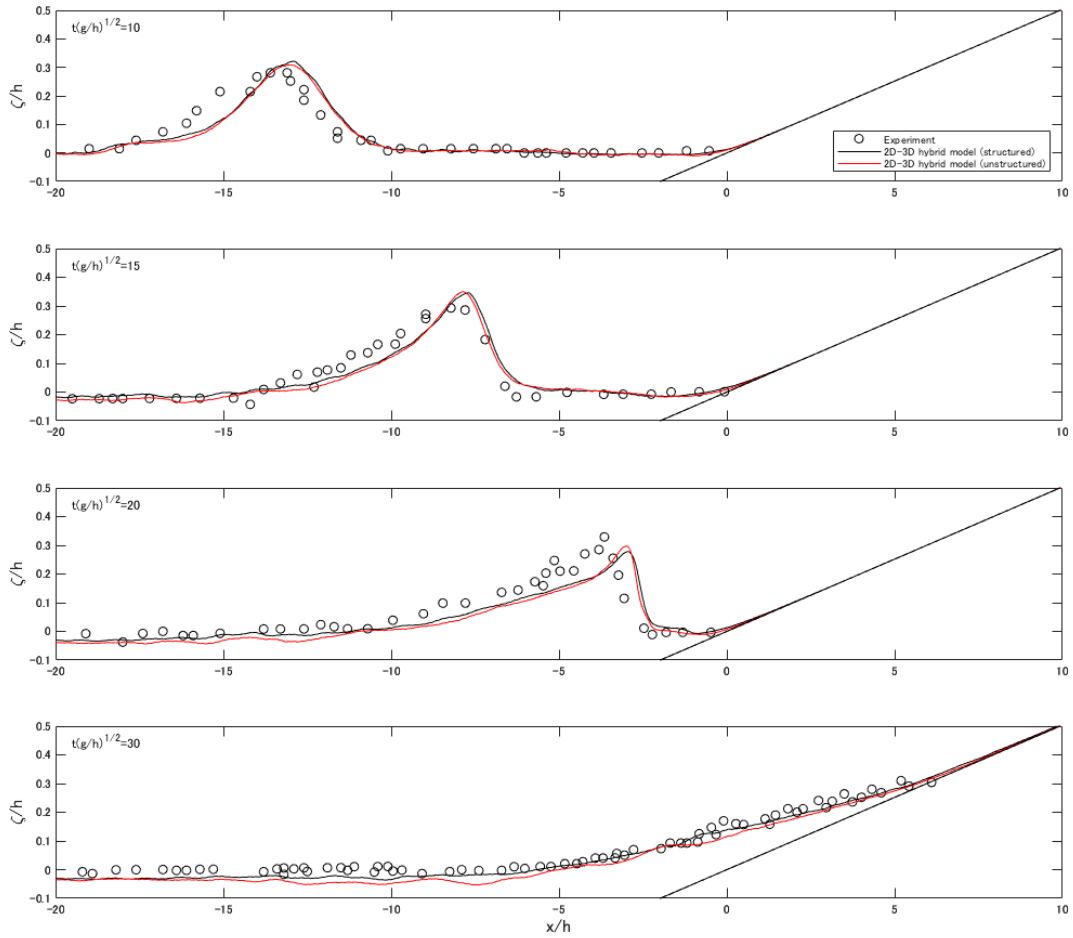

FIGURE 13 Comparison of surface profiles.

and unstructured mesh shown in **Figure 12** are compared. Case 2 examines a different position of the overlap domain. The results are compared with experimental results[21] and those from fully 2D and fully 3D analysis models. For the initial conditions, the initial wave height is set to

$$\zeta(x, t = 0) = \frac{\zeta_0}{h}\mathrm{sech}^2\sqrt{\frac{3\zeta_0}{4h}}(x - x_0), \tag{25}$$

where the ratio of wave height ζ_0 to depth h is 0.3. x_0 is the location of the wave crest. The initial flow velocity is set by the following equation:

$$u(x, t = 0) = \zeta(x, t = 0)\sqrt{\frac{g}{h}}. \tag{26}$$

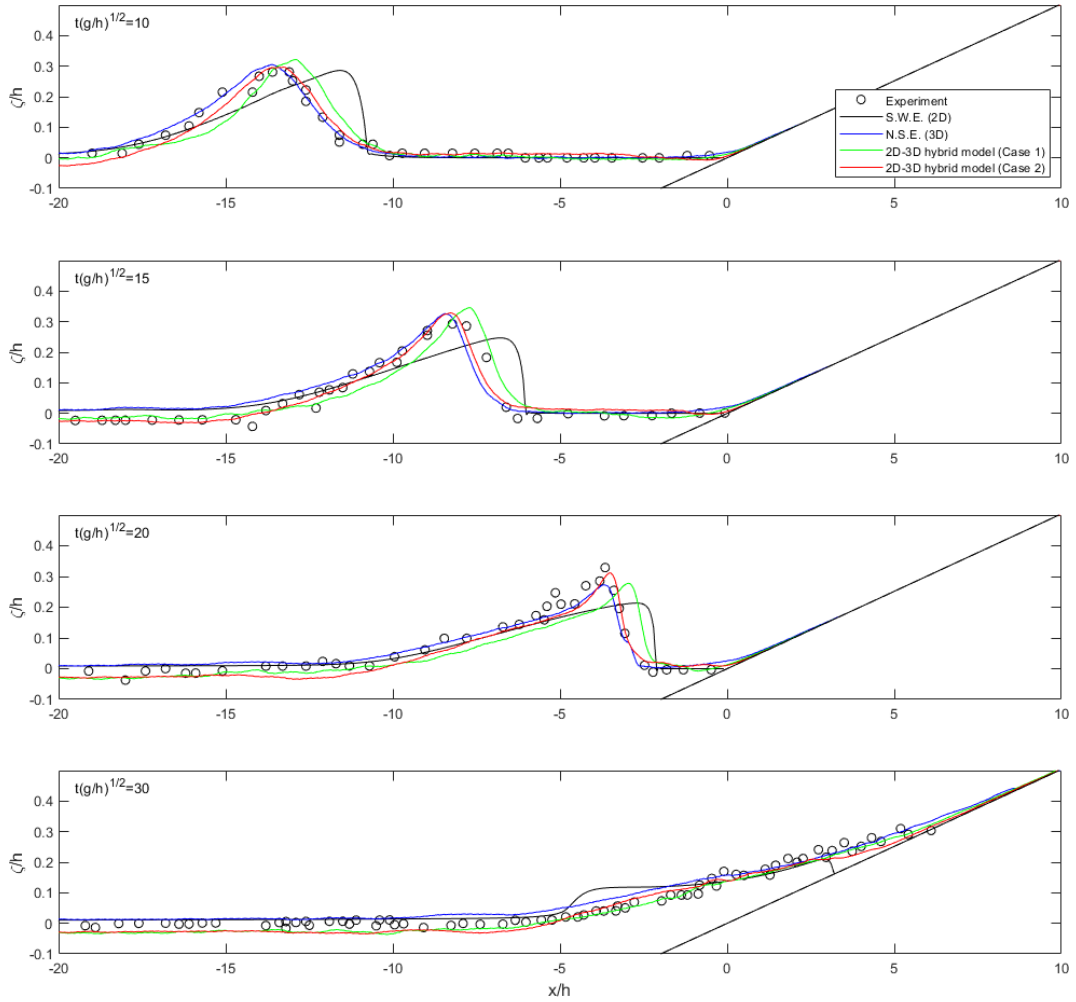

FIGURE 14 Comparison of surface profiles.

The wave crest is located at half of the solitary wavelength from the front end of the slope.

$$L = \sqrt{\frac{4h}{3\zeta_0}}\operatorname{arccosh}\left(\sqrt{\frac{1}{0.05}}\right). \tag{27}$$

Figure 12 shows the meshes around the connection boundary. In case 1, the mesh size is set to 0.05 m, and the width of the overlap domain is 0.2m (four elements). For a comparison with the case1 and case 2, a fully 2D and a fully 3D simulations were implemented by using structured meshes. The slip boundary condition is applied on the wall and the bottom. The kinematic viscosity coefficient ν_e is set to 1.0×10^{-3} m^2/s, and Manning's roughness coefficient n is set to $0.01\mathrm{s}/\mathrm{m}^{\frac{1}{3}}$ for the 2D analysis.

The surface profiles for case 1 at different dimensionless times ($t' = t\sqrt{\frac{g}{h}} = 10, 15, 20, 30$) are compared in **Figure 13**, where the circles denote the experimental results and the lines denote the results from the 2D-3D hybrid model. From the figure, the difference in using the structured mesh or the unstructured mesh for the 2D-3D hybrid model is negligible, and the computational results are generally consistent with the experimental results. **Figure 14** compares cases 1 and 2. In the figure, S.W.E. denotes the result given by solving the 2D shallow water equations and N.S.E. denotes the result given by solving the 3D Navier-Stokes equations. From the figure, we can see the results of case 2 are close to those of the 3D model, and they exhibit better agreement with the experimental results than the results of case 1 and the 2D model, which is because the case 2 gets less wave transformation effect by the 2D shallow water model. **Figure 15** shows snapshots of the free surfaces (scales have been changed for clearer visualization) at $t = 2.5$ s, from which we can see that the computational results are stable.

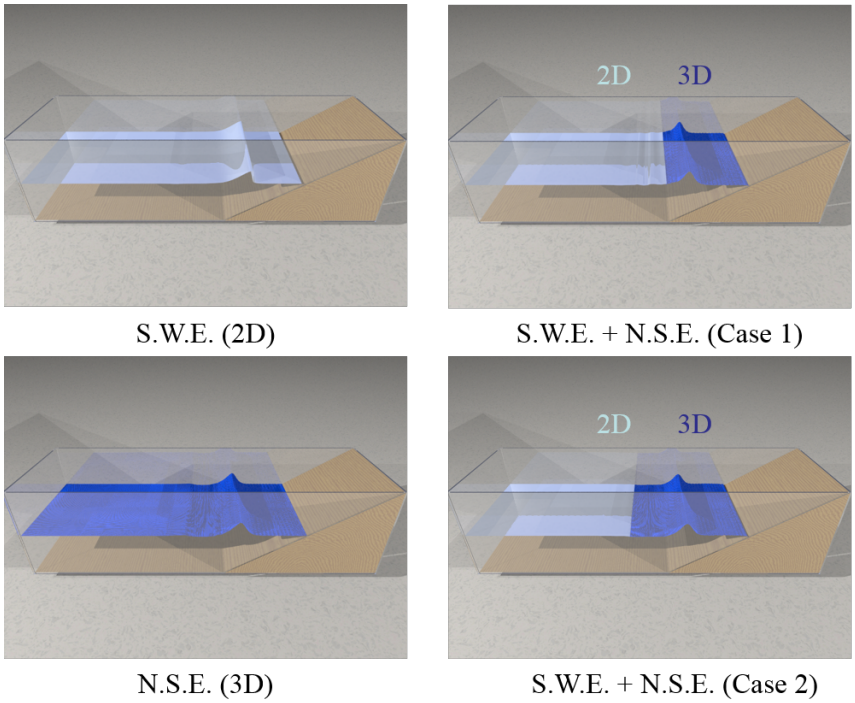

FIGURE 15 Snapshots of surface profiles at t=2.5s.

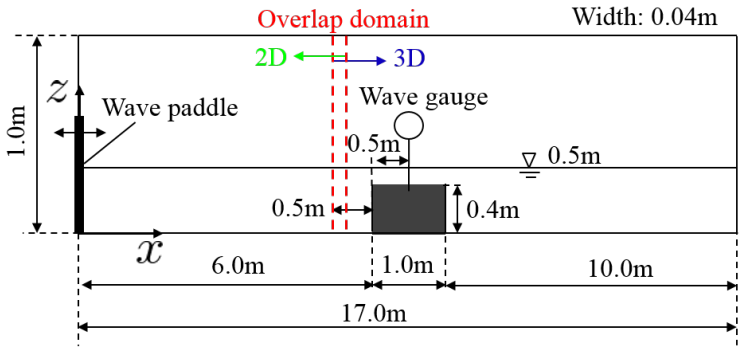

FIGURE 16 Computational model.

6.3 | Wave motion around a submerged breakwater

To investigate the effectiveness and influence of the width of the overlap domain in the proposed 2D-3D hybrid model, the wave motion around a submerged breakwater (**Figure 16**) is simulated. In this problem, a wave maker is positioned on the left side of the model. Two cases of Cnoid waves are considered. For case A, the wave height is 0.05 m and the period is 2.0 s. For case B, the wave height is 0.075 m and the period is 1.0 s. For the computational conditions, the mesh size of the 2D domain is 0.01 m. In the 3D domain, the mesh around the breakwater has dimensions of 0.01 m and that in other region has a size of 0.02 m (see **Figure 17**). The slip boundary condition is applied on the wall of the aquarium, and the time increment is 0.001 s.

Figure 18 shows the time history of water level variation at the wave gauge for comparing the width of the overlap domain for the two waves. In the figures, the circles denote the experimental results, and each solid line shows the result for a different width of the overlap domain. For case A, we can see that all the numerical results are in good agreement with the experimental results[22]. For case B, an overlap domain of more than 0.04 m (four elements) produces better agreement with the experimental results than an overlap of 0.01 m (one element) or 0.02 m (two elements). In conclusion, it is preferable to use more than four elements for the width of the overlap domain, but considering the computational cost, four elements are considered to be

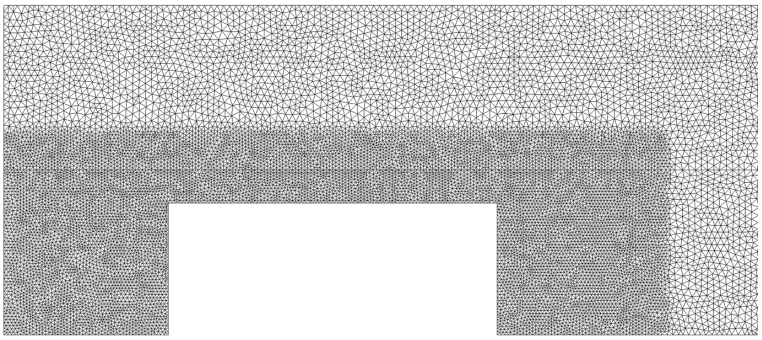

FIGURE 17 Mesh around the breakwater.

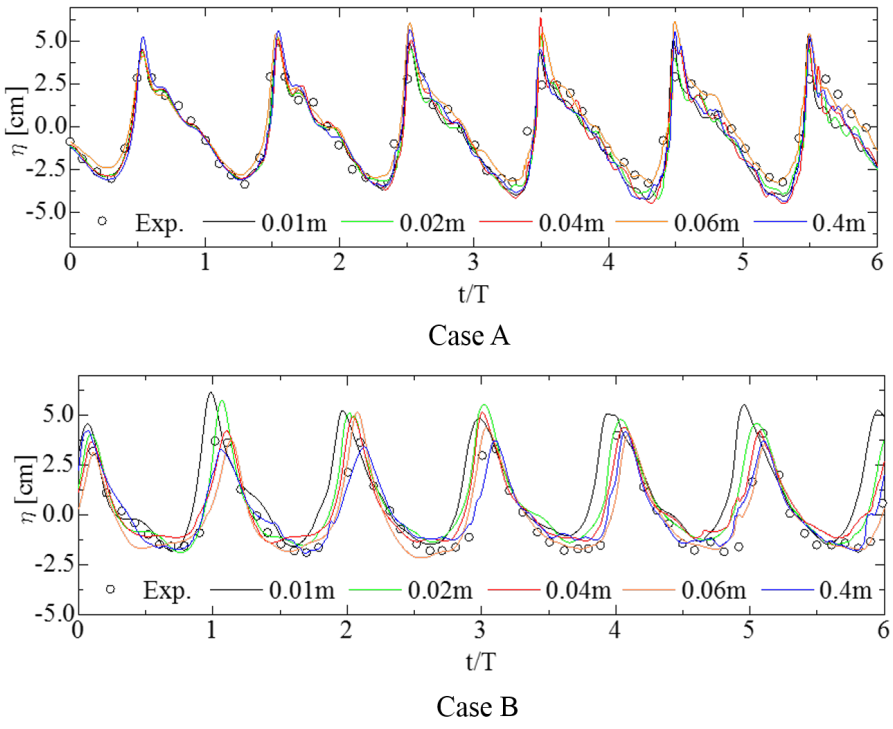

FIGURE 18 Time history of water level variation for the comparison of the width of the overlap domain.

sufficient. **Figure 19** shows the time history of the water level variation at the wave gauge for the 2D model and the 2D-3D hybrid model for case A. In the figure, the circles denote the experimental results, the black line denotes the result given by the fully 2D model governed by S.W.E., and the red line denotes the result given by the 2D-3D hybrid model (overlap domain with four elements). From the comparison, we can see that using the 2D-3D hybrid model provides better agreement with the experimental results than the 2D model.

6.4 | Dam-break with structures

Figure 20 shows two computational models to test the performance of the 2D-3D hybrid model. In this test, the proposed switch method is applied, both of the computational models are computed by the 2D at first before the wave propagating to the 3D domain. Then when the wave reaches the 3D domain, the hybrid model begins to work. For the 3D domain, the Case A is set as a square, the Case B is set as a diamond shape, which is to show the optionality of the shape choosing for the 3D domain. For the computational conditions, the mesh size of the 2D domain is 0.1m and the mesh size of the 3D domain is 0.05m, The coupling

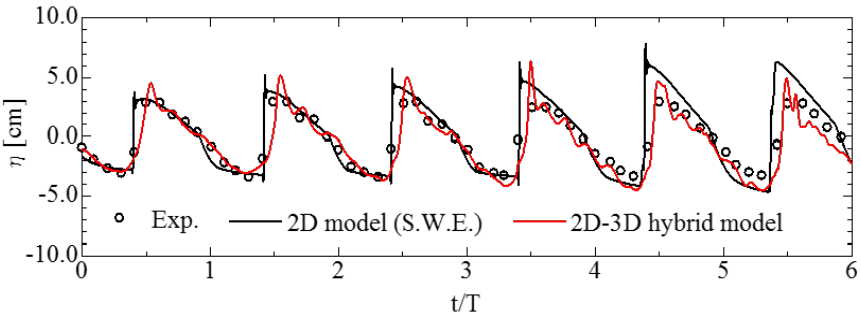

FIGURE 19 Time history of water level variation using the wave of case A.

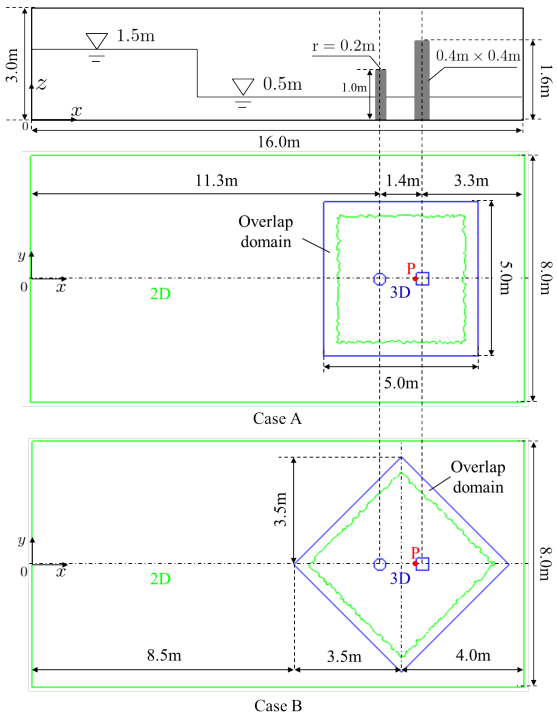

FIGURE 20 Computational model.

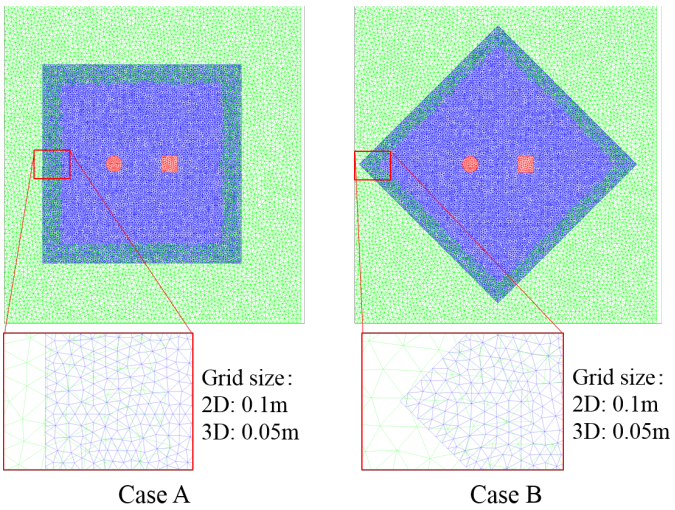

FIGURE 21 Computational mesh around the overlap domain.

domain is set to be 0.4m (four 2D elements, see **Figure 21**). The time increment is 0.001s and the slip boundary condition is applied.

Several snapshots of surface profiles are shown in **Figure 22**. From these figures, we can see from $t = 0.80$s to $t = 2.25$s, the 2D analysis model changes into 2D-3D hybrid model when the wave reaches the 3D domain. We can also confirm that the 2D-3D hybrid model solve this computational problem stably. **Figure 23** shows the time history of water depth variation at P(12.5, 0.0), we can see both the results are almost the same. The arbitrary choices of the 3D domain and the grids have been shown.

7 | CONCLUSIONS

In this paper, a two-way coupling 2D-3D hybrid tsunami model using the overlapping method has been developed. In this model, a 2D shallow water model is applied for the purpose of simulating tsunami waves propagate from source area to offshore area,

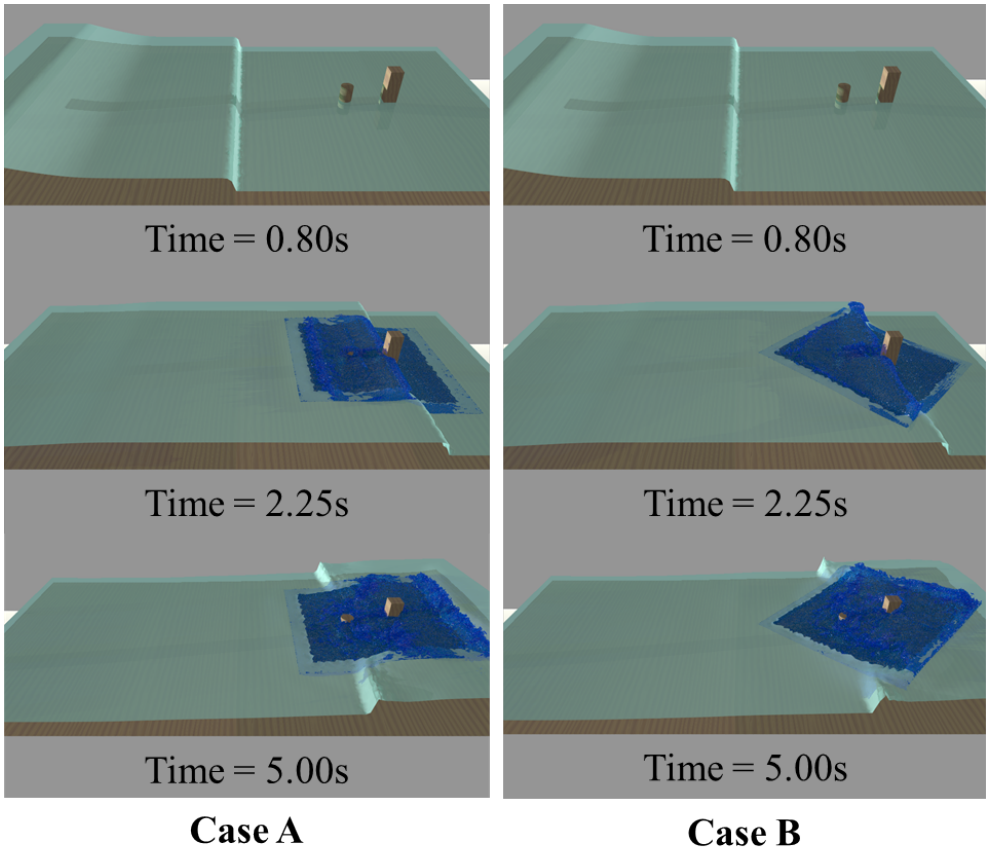

FIGURE 22 Snapshots of surface profiles.

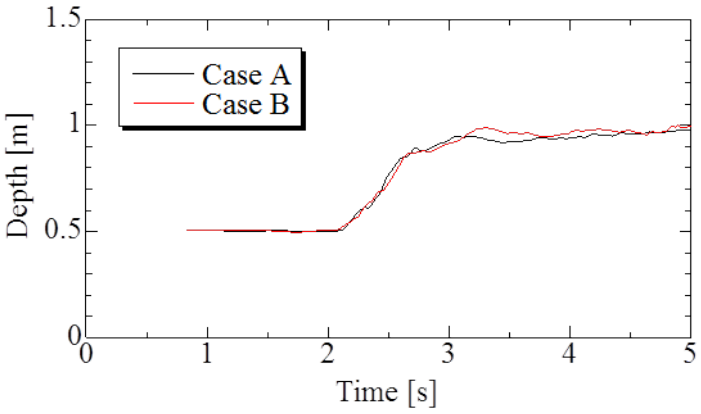

FIGURE 23 Time history of water depth variation at P(12.5, 0.0).

a 3D free surface flow model using Phase-Field Model based on Allen-Cahn equation is applied for the purpose of capturing accurate interface of the water in the target coastal area with structures, and both models are based on the stablized finite element method. The overlapping method that satisfies the conservation and compatibility conditions was proposed to couple the 2D and 3D models. Moreover, a switch method for the purpose of further increase the efficiency of the 2D-3D coupling method was

proposed. To demonstrate the accuracy and applicability of the present model, a series of numerical examples have been tested, and the following conclusions can be drawn:

- The results for the rotating cylinder problem show that Allen-Cahn equation retains the interface for the advection problem better compared to the pure advection equation, and reduces the overshoot and undershoot.
- From the solitary wave run-up problem, the results of the 2D-3D hybrid model are in better agreement with the experimental results than the results of the 2D model. The 2D-3D hybrid model is suitable for use with both structured and unstructured meshes.
- Simulations of the wave motion around a submerged breakwater demonstrate that choosing the width of the overlap domain to be four elements produces reasonable results. Additionally, the results of the 2D-3D hybrid model exhibit better agreement with the experimental results than the results of a fully 2D model.
- The test of dam-break with structures show the advantage of the proposed 2D-3D hybrid method that the shape of 3D domain can be set arbitrary, and the potential of increasing efficiency for the large-scale tsunami simulation by the proposed switch method.

Future work will be focused on applying the present method to large-scale tsunami simulations over real terrain, and evaluate the accuracy and efficiency of the presented model by comparing model results to station observations.

ACKNOWLEDGMENTS

This work was supported by JSPS KAKENHI Grant Number 18K04665.

References

1. Imamura F, Yalciner A, Ozyurt G. Tsunami modelling manual (Tsunami model). *UNESCO IOC international training course on Tsunami Numerical Modelling* 2006. URL:https://www.tsunami.irides.tohoku.ac.jp/hokusai3/J/projects/manual-ver-3.1.pdf, Accessed November 21, 2022.
2. Takase S, kashiyama K, Tanaka S, Tezduyar T. Space-time SUPG formulation of the shallow-water equation. *International Journal for Numerical Methods in Fluids* 2010(64): 1379–1394. DOI:https://doi.org/10.1002/fld.2464.
3. Kanayama H, Dan H. A tsunami simulation of Hakata Bay using the viscous shallow-water equations. *Japan Journal of Industrial and Applied Mathematics* 2013(30): 605–624. DOI:https://doi.org/10.1007/s13160-013-0111-7.
4. Liu Y, Shi Y, Yuen D, Sevre E, Yuan X, Xing H. Comparison of linear and nonlinear shallow wave water equations applied to tsunami waves over the China Sea. *Acta Geotechnica* 2009(4): 129–137. DOI:https://doi.org/10.1007/s11440-008-0073-0.
5. Shijo R, Tsukuda Y, Sato T, et al. Tsunami simulation by 3D model around a power station due to the 2011 Tohoku earthquake. In: . 58. ; 2016: 1640014-1–1640014-18. DOI:https://doi.org/10.1142/S0578563416400143.
6. Isshiki M, Asai M, Eguchi S, O-Tani H. 3D tsunami run-up simulation and visualization using particle method with Gis-Based geography model. In: . 10. ; 2016: 1640020. DOI:https://doi.org/10.1142/S1793431116400200.
7. Masamura K, Fujima K, Goto C, Iida K, Shigemura T. Numerical analysis of tsunami by using 2d/3d hybrid model (in Japanese). *Journal of JSCE* 2001(2001(670)): 49–61. DOI:https://doi.org/10.2208/jscej.2001.670_49.
8. Tomita T, Kakinuma T. Storm surge and tsunami simulation in oceans and coastal areas (STOC) (in Japanese). *Report of the Port and Airport Research Institute* 2005(44(2)): 83–98. URL:https://www.pari.go.jp/search-pdf/vol044-no02-05.pdf, Accessed November 21, 2022.
9. Fukui T, Koshimura S, Matsuyama M. 2D-3D Hybrid Simulation of Tsunami Inundation Flow by Lattice Boltzmann Method (in Japanese). *Journal of Japan Society of Civil Engineers* 2010; 66(1): 61–65. DOI:https://doi.org/10.2208/kaigan.66.61.

10. Pringle W, Yoneyama N, Mori N. Two-way coupled long wave - RANS model: Solitary wave transformation and breaking on a plane beach. *Coastal Engineering* 2016; 114: 99–118. DOI:https://doi.org/10.1016/j.coastaleng.2016.04.011.

11. Arikawa T, Tomita T. Development of High Resolution Tsunami Runup Calculation Method Based on a Multi Scale Simulation (in Japanese). *Report of the Port and Airport Research Institute* 2014; 53(2): 3–18. URL:https://www.pari.go.jp/search-pdf/houkokuVol53-2.pdf, Accessed November 21, 2022.

12. Takase S, Moriguchi S, Terada K, et al. 2D-3D hybrid stabilized finite element method for tsunami runup simulations. *Comput. Mech.* 2016; 58: 411–422. DOI:https://doi.org/10.1007/s00466-016-1300-4.

13. Mitsume N, Donahue A, Westerink J, Yoshimura S. Coupling methods between finite element-based Boussinesq-type wave and particle-based free-surface flow models. *International Journal for Numerical Methods in Fluids* 2018; 88: 141–168. DOI:https://doi.org/10.1002/fld.4516.

14. Asai M, Miyagawa Y, Idris N, Muhari A, Imamura F. Coupled tsunami simulations based on a 2D shallow-water equation-based finite difference method and 3D incompressible smoothed particle hydrodynamics. *Journal of Earthquake and Tsunami* 2016; 10(5): 1640019. DOI:https://doi.org/10.1142/S1793431116400194.

15. Hirt C, Nichols B. Volume of fluid (VOF) method for the dynamics of free boundaries. *Journal of Computational Physics* 1981; 39(1): 201–225. DOI:https://doi.org/10.1016/0021-9991(81)90145-5.

16. Kawahara M, Umetsu T. Finite element method for moving boundary problems in river flow. *International Journal for Numerical Methods in Fluids* 1986; 6: 365–386. DOI:https://doi.org/10.1002/fld.1650060605.

17. Beaucourt J, Biben T, Leyrat A, Verdier C. Modeling breakup and relaxation of Newtonian droplets using the advected phase field approach. *Physical Review E* 2007; 75: 021405(1–8). DOI:https://doi.org/10.1103/PhysRevE.75.021405.

18. Matsumoto J, Sawada T. A Study on Mobility of Gas-Liquid Two-Phase Flow using Phase-Field Model [in Japanese]. *Proceedings of the Conference on Computational Engineering and Science* 2017; 22. URL:https://iss.ndl.go.jp/books/R000000004-I026500143-00?ar=4e1f&locale=en, Accessed November 21, 2022.

19. Matsumoto J, Takada N. Two-phase flow analysis based on a phase-field model using orthogonal basis bubble function finite element method. *International Journal of Computational Fluid Dynamics* 2008; 22(8): 555–568. DOI:https://doi.org/10.1080/10618560802238226.

20. Tezduyar T. Stabilized finite element formulations for incompressible flow computations. *Advance in applied Mechanics* 1991; 28: 1–44. DOI:https://doi.org/10.1016/S0065-2156(08)70153-4.

21. Synolakis C. The runup of solitary wave. *Journal of Fluid Mechanics* 1987; 185: 523–545. DOI:https://doi.org/10.1017/S002211208700329X.

22. Sakuraba M, Kashiyama K. Free surface flow using levelset method based on stablized finite element method (in Japanese). *Proceedings of Coastal Engineering, JSCE* 2003; 50: 16–20. DOI:https://doi.org/10.2208/proce1989.50.16.